

Liquefaction triggering and post-liquefaction deformation of laminated deposits

Panagiota Tasiopoulou^{a,*}, Amalia Giannakou^a, Jacob Chacko^a, Sjoerd de Wit^b

^a *Fugro, Turkey*

^b *Shell Global Solutions International B.V., Netherlands*

ARTICLE INFO

Keywords:

Laminated soils
Liquefaction
Cyclic tests
Void redistribution
Deformation accumulation

ABSTRACT

As part of dynamic stability evaluations of earth embankments founded on laminated sand and clay deposits, the need to characterize their cyclic resistance became critical for the assessment of the embankment behavior and subsequent decisions on liquefaction mitigation measures. Due to lack of experimental and case history data on the effective stress behavior of such deposits, which are typically encountered in tidal and alluvial depositional environments, advanced laboratory tests on high quality undisturbed samples and numerical simulations using advanced constitutive models were performed to gain insight on liquefaction triggering and post-liquefaction accumulation of deformations under level and sloping ground conditions of such formations. Results indicated that the presence of clay laminations within sand deposits tends to increase the liquefaction triggering resistance. The increase in liquefaction resistance becomes more pronounced as the percentage of clay laminations increases. Numerical analyses results also indicated that void redistribution effects, often related to strain localization effects, tend to reduce as the thickness of sand laminations decreases, or as the clay lamination percentage increases.

1. Introduction

Performance-based concepts are increasingly used in earthquake engineering design practice. Nonlinear deformation analyses, involving dynamic finite element or finite difference methods, are frequently used for evaluating the effects of liquefaction on embankment dams and other major soil-structure systems during earthquakes.

In engineering practice, the response of a geotechnical structure to strong ground motion is typically evaluated by means of empirical equations developed using either simplified system models or available observations from well-documented case histories. Despite their ease of use, empirical models may be overly simplistic in characterizing the response of complex systems and may not capture important phenomena associated with earthquake problems. In the context of performance-based design, numerical analyses combined with advanced cyclic testing for the calibration of constitutive models can offer an alternative, refined response model compared to simplified algebraic equations.

Existing simplified procedures [1–4] used for liquefaction assessment mainly focus on evaluating liquefaction triggering and post-liquefaction residual strength of sands based on in situ tests (i.e. CPT tip resistance or SPT blowcounts). In intertidal or alluvial environments, however, coarse-grained materials are frequently encountered within

thinly layered deposits comprising alternating thin laminations of sands and clays. (Fig. 1). In such deposits, liquefaction assessment based on empirical correlations with CPT tip resistance may not be applicable due to the effect of the clay laminations on the CPT tip resistance measured within the thin “sandwiched” sand layers. An example CPT log in laminated sand and clay deposits including measured tip resistance, q_c , friction ratio, R_f , pore water pressure response, u_2 and soil behavior interpretations based on Robertson [5] soil classification is demonstrated in Fig. 2. Because the sand layers within the interlayered deposits are thin (perhaps 1–20 cm thick) the tip resistances do not fully develop to a level that would provide a meaningful representation of the soil density. However, the signature of the CPT data which is essentially showing an averaged response of multiple layers is often similar to that of a loose silty sand or a sandy silt. Due to this influence of the fine-grained laminations on tip resistance, simplified liquefaction triggering correlations based on CPT data cannot be reliably used to assess the liquefaction potential of such deposits.

For dynamic stability evaluations of earth embankments founded on laminated sand and clay deposits, quantifying their cyclic resistance is critical for assessment of embankment behavior and subsequent decisions on mitigation measures. While extensive research has been conducted on the liquefaction resistance of intermediate soils and sand materials mixed with fines [6–13], there is a lack of experimental and

* Corresponding author.

<https://doi.org/10.1016/j.soildyn.2018.04.044>

Received 25 September 2017; Received in revised form 29 March 2018; Accepted 25 April 2018
0267-7261/ © 2018 Elsevier Ltd. All rights reserved.

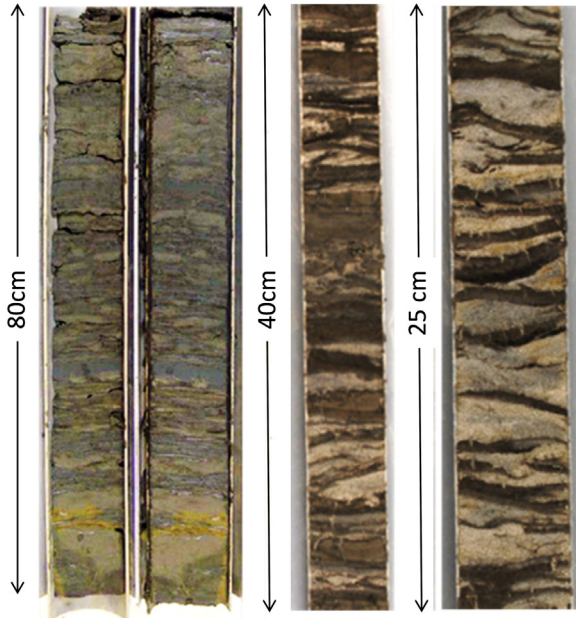


Fig. 1. Tubes of laminated deposits with alternating thin layers of sand and clay.

case history data on the cyclic behavior of layered soil deposits. To overcome this, advanced cyclic laboratory tests on high quality undisturbed laminated samples and numerical simulations using advanced constitutive models were performed to gain insight on liquefaction triggering and post-liquefaction accumulation of deformations under level and sloping ground conditions. These results provided the basis for the selection of representative properties and calibration of constitutive models used in 2D dynamic stability numerical evaluations of earth embankments founded on laminated deposits.

2. Advanced cyclic testing

A series of stress controlled Cyclic Direct Simple Shear (CDSS) and Cyclic Triaxial (CTX) tests was performed on “undisturbed” samples obtained from laminated deposits. The purpose of the tests was to estimate the liquefaction triggering and post-liquefaction shear deformation potential of these formations. Due to the presence of a levee, cyclic tests were conducted for two cases: 1) Without initial static shear stress (no static bias), and 2) With initial static shear stress (static bias on the order of 0.2). To obtain high quality samples, conventional and advanced sampling techniques such as Piston and Gel-Push sampling were used. While Piston sampling has long been used in the industry, the latter was recently developed as a method to better retain natural in-situ soil structure and was successfully applied in Japan, Taiwan and New Zealand [14–16]. The advantage of Gel-Push sampling over more conventional techniques is the injection of a water-soluble diluted polymer to reduce the friction between the sample and the core liner tube as the sample is pushed into the ground. The fluid thus minimizes disturbance both during sample collection and extrusion.

The cyclic test results were used to evaluate the liquefaction resistance of individual sand layers within the laminated deposits where CPT tip resistance may have been impacted by the presence of adjacent soft layers and to calibrate nonlinear effective-stress constitutive models that were used to simulate the composite behavior of laminated deposits under earthquake loading in numerical evaluations.

2.1. Sample selection

In order to facilitate sample selection, Multi-Sensor Core Logging (MSCL-S) and X-ray radiography were initially performed on selected tubes to identify suitable undisturbed subsamples for advanced cyclic testing. On the X-ray results shown on Fig. 3, lower density fine-grained laminations can be identified with the lighter colors (closer to white), as opposed to higher density coarse-grained layers depicted with darker colors (typically grey or almost black).

Disturbance of soil samples obtained from the field was evaluated in order to determine the degree to which the test results performed on the undisturbed samples were representative of in-situ conditions. While

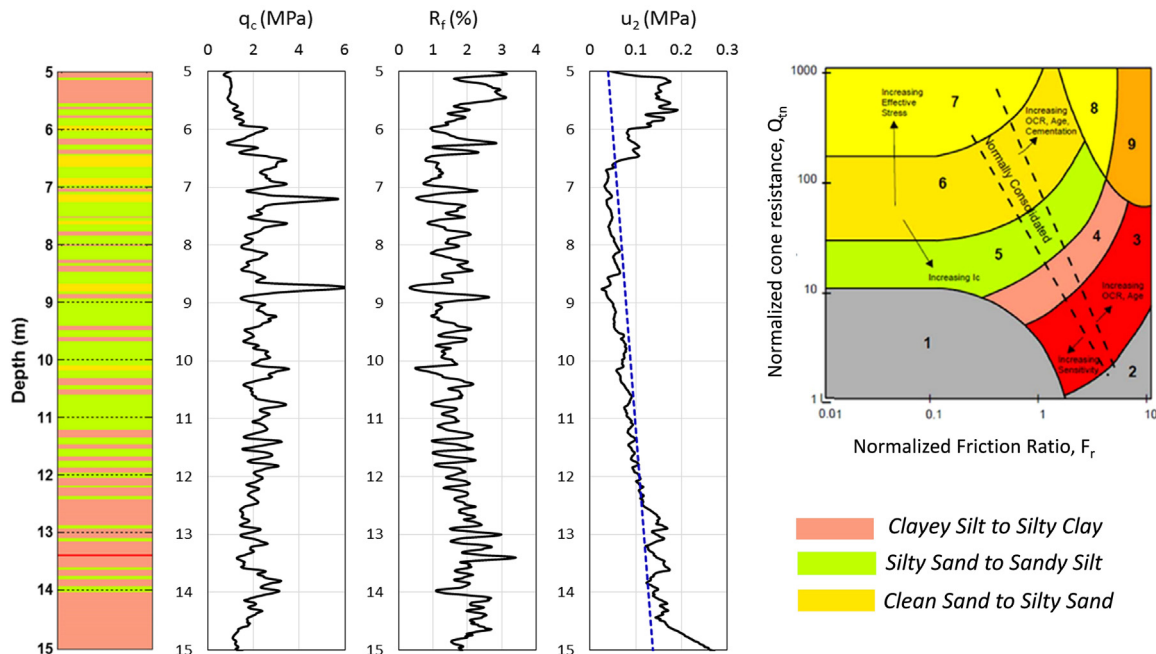


Fig. 2. Example CPT log in laminated sand and clay deposits showing tip resistance, q_c , friction ratio R_f , pore water pressure response, u_2 along with the hydrostatic pressure (blue dashed line) and soil classification per Robertson [5].

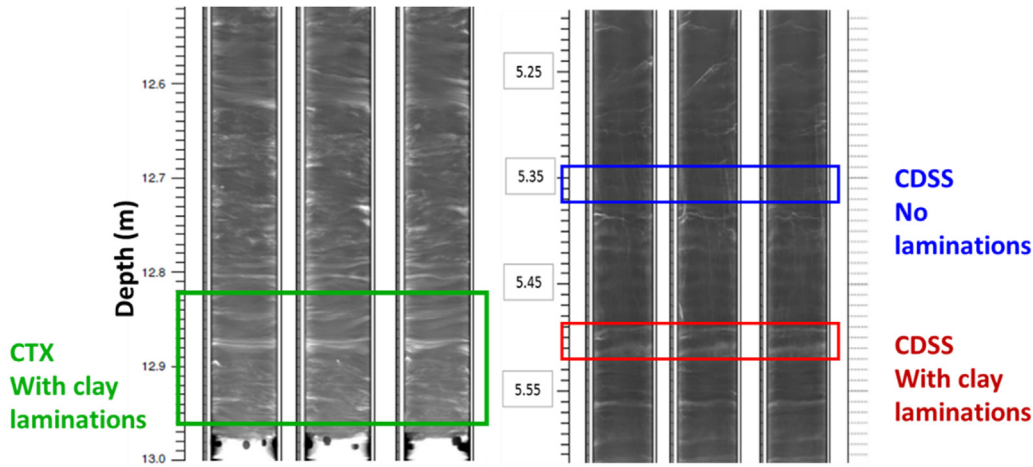


Fig. 3. Examples of sample selection for CDSS and CTX testing based on X-ray radiography.

there is no direct measurement of sample disturbance, a number of indirect methods have been attempted by other researchers [17] to quantify sampling disturbance including assessments of changes in sample density and soil small strain stiffness.

For this study sample disturbance was evaluated through comparison between: (i) in-situ shear wave velocity measurements from Seismic CPTs (i.e. SCPTs) and measured shear wave velocity from bender element tests in the laboratory and (ii) density from MSCL-S tomography (i.e. before sample extrusion) and measurements of bulk density of the tested samples in the laboratory (i.e. after sample extrusion). Both the shear wave velocity data, and the density data suggest that there was some loosening of the samples that were tested. This implies that the cyclic resistance obtained by laboratory testing may be underestimated compared to the in situ one, especially in case of the uniform sand samples.

Individual sand layers within the tidal deposits were targeted for the stress-controlled CDSS tests due to the small size of the specimen (i.e. ~ 3 cm), while laminated sand and clay materials were targeted for CTX tests where specimen size (i.e. ~ 14 cm) is large relative to the thickness of the clay laminations (typically 1–2 cm thick). Where possible, sand samples including even thinner clay laminations were tested in CDSS tests. Typical examples of CDSS and CTX sample selection from MSCL-S and X-ray results are shown on Fig. 3. Fig. 4 depicts indicative particle size distribution curves for the three types of specimens selected for laboratory testing, shown on Fig. 3. It is evident that the specimens containing clay laminations exhibit higher fines content. For comparison, ranges of particle size distribution for Nevada sand [18,19] and a soft clay from Adapazari, Turkey [20] were also plotted on Fig. 4.

2.2. Liquefaction triggering from cyclic test results

CTX and CDSS tests were performed using GDS equipment at mean effective stresses ranging from 80 to 120 kPa and at cyclic frequencies between 0.1 and 1 Hz. Initially, the samples were extruded from the sample tube and carefully trimmed to specific dimensions according to test-specific requirements. The specimens were weighed and measured to determine the bulk density, while a moisture content determination was carried out on a portion of soil trimmings representative of the specimen to be tested, allowing for an estimate of the initial air-voids in the specimen. After the placement of the specimens in the GDS apparatus three basic stages were performed: i) saturation of the specimen, ii) consolidation to the required stress level maintaining the specimen saturation and allowing sufficient time for equalization of pore pressures within the specimen and iii) cyclic loading. Table 1 provides information on the performed cyclic tests.

Initially, a number of cyclic tests was performed at a frequency of

1 Hz, which is commonly used for earthquake applications. Keeping in mind that most of the tested specimens are not homogeneous and even the uniform sand samples contain about 20% fines, as indicated by the particle-size distribution on Fig. 4, subsequent cyclic tests were performed at lower frequencies, such as 0.5 Hz and 0.1 Hz in order to investigate the effect of loading rate on the response of these type of soils. In general, consistency and repeatability of the soil response was confirmed when comparing the test results obtained from different frequency levels. Specific observations on effective stress paths for different frequencies showed that, in some cases, zero-effective stress was not reached despite the development of a failure envelope with the characteristic “butterfly” shape accompanied by deviatoric strains larger than 3%. This “drift” in the measured effective stress seems associated with: a) the fines content of the sand layers, b) the existence of clay laminations within the specimen, and c) given the non-homogeneity of most samples, the location where the pore water pressure is measured during the test (e.g. in the case of CTX tests, the pore water pressure is measured at the base of the specimen) which may not capture a non uniform pore pressure field. Similar stress paths have been reported in the literature from CSS tests on samples with fines content ([13], [21,22]). Moreover, Bray and Sancio [12] performed CTX tests on fine-grained soils (Adapazari clay) at frequencies of 1 Hz and 0.005 Hz and observed the effective stress paths. For the 1 Hz tests, zero effective stress was not achieved despite the development of large axial strains indicative of liquefaction, while for the 0.005 Hz tests, zero effective stress values were observed during loading. Despite this discrepancy, they concluded that liquefaction resistance curves estimated for each loading frequency were consistent when a strain criterion was used to assess liquefaction triggering.

Fig. 5 depicts the Cyclic Stress Ratio (CSR) as a function of the number of cycles required to trigger liquefaction, obtained from CDSS and CTX tests performed on uniform and laminated samples without static bias. Liquefaction triggering is considered to occur at 3% Single-Amplitude shear strain for the CDSS tests and 1.5–2% Single-Amplitude axial strain for the CTX tests. CSR for CDSS tests is defined as the ratio of maximum applied shear stress over the initial vertical effective stress, while CSR for CTX tests is equal to the difference between the maximum and minimum principal stresses divided by two, over the initial mean effective stress. It should be noted that no conversion factor has been applied to the CSRs of the CTX tests on laminated samples plotted on Fig. 5.

Due to the variable nature of the intertidal deposits, it is practically impossible to target identical samples with the same initial void ratio, relative density or percentage of clay laminations for cyclic testing at multiple cyclic stress ratios. Therefore, the laminated samples cannot be characterized in terms of relative density since direct measurement of

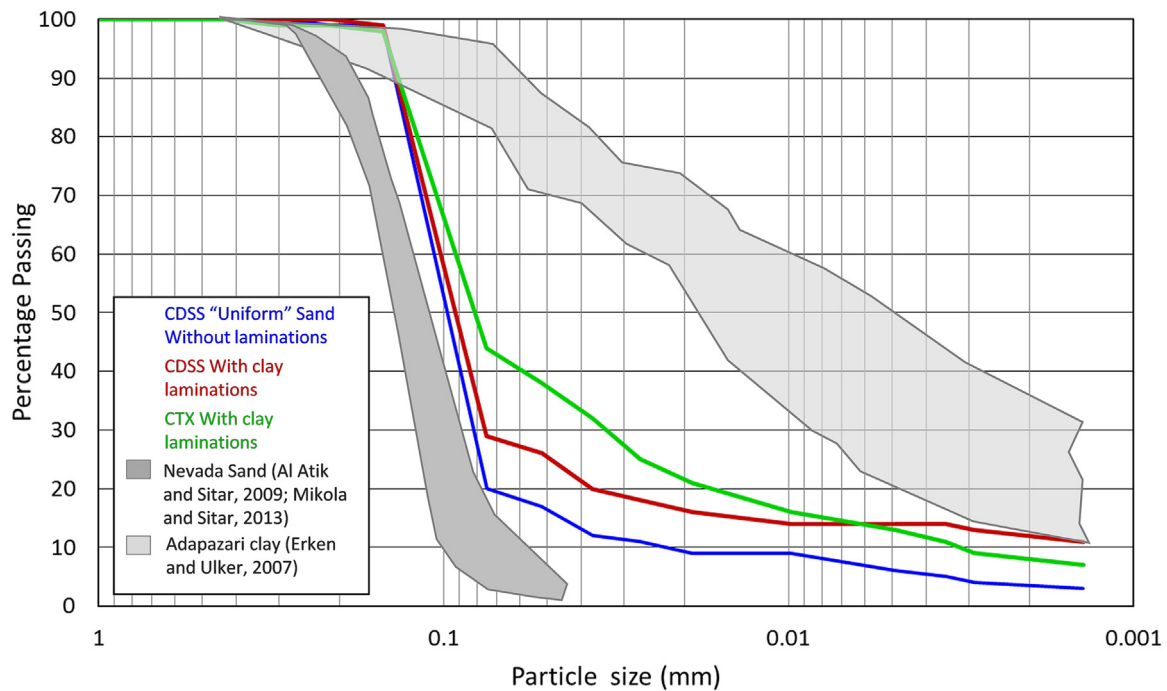


Fig. 4. Indicative particle size distribution curves (blue, red and green) of the three types of specimen selected for laboratory testing, shown on Fig. 3. Grey areas correspond to Nevada sand [18,19], and to a soft clay from Adapazari, Turkey [20].

Table 1
Summary of performed cyclic laboratory tests.

Type of testing	Sample description	Sampling technique	e_0^a	Degree of saturation (%) ^a	Vertical effective stress (kPa) ^a	Loading frequency (Hz)	Cyclic stress ratio (CSR)
CDSS	uniform sand	Gel Push	0.65	99	100	0.1	0.13
CDSS	uniform sand	Gel Push	0.66	98	80	0.1	0.138
CDSS	uniform sand	Gel Push	0.65	97	100	0.5	0.17
CDSS	uniform sand	Piston	0.69	97	80	1	0.088
CDSS	uniform sand	Piston	0.67	100	120	1	0.183
CDSS	laminated	Gel Push	0.77	100	80	1	0.175
CDSS	laminated	Gel Push	0.84	97	80	1	0.188
CDSS	laminated	Piston	0.83	95	120	1	0.1
CDSS	laminated	Piston	0.78	94	80	1	0.15
CDSS	laminated	Piston	0.81	99	80	1	0.2
CTX	laminated	Piston	0.85	100	115	1	0.142
CTX	laminated	Piston	0.86	100	115	1	0.28
CTX	laminated	Piston	0.86	100	120	1	0.305
CTX	laminated	Gel Push	1.06	100	120	0.5	0.358
CTX	laminated	Gel Push	1.02	100	80	0.5	0.35
CTX	laminated	Gel Push	0.91	100	120	0.1	0.183
CTX	laminated	Gel Push	0.89	85	120	0.1	0.42
CTX	laminated	Piston	1.21	100	100	1	0.1
CTX	laminated	Piston	1.00	100	100	1	0.15
CTX	laminated	Piston	1.12	100	100	1	0.3

^a After consolidation stage, prior to cyclic loading.

minimum/maximum density is not feasible for each sample. In order to provide a basis for identifying similar samples and to develop reasonable cyclic liquefaction resistance curves, the initial sample void ratio after the consolidation stage was used as an indicator and is plotted next to each test on Fig. 5. As shown on this figure most of the tested samples have different initial void ratios. These void ratio values provide an indication of the sand/clay lamination analogy within the sample: usually, the higher the initial void ratio, the higher the clay

lamination percentage within the sample. Based on this and the sample-selection concept described in Section 2.2, the low-range values of the initial void ratio are indicative of uniform sand samples without clay laminations. Higher values of initial void ratio suggest the presence of clay laminations within the samples.

Interpreted liquefaction resistance curves (plotted with the coloured solid and dashed lines on Fig. 5) were developed from CDSS and CTX test results. The lower liquefaction resistance curve (blue) corresponds to uniform sand samples (non-laminated) subjected to CDSS loading with an indicative initial void ratio equal to 0.65 approximately. The intermediate red curve represents laminated samples subjected to CDSS loading with an average initial void ratio close to 0.8. The dashed and solid green curves demonstrate the liquefaction resistance of laminated samples subjected to CTX loading with a representative void ratio close to 0.86 and 1, respectively. In substance, the interpreted laboratory results plotted on Fig. 4 indicate that the presence of clay laminations in the samples (red and green curves) leads to an increase in liquefaction triggering resistance compared to a uniform sand sample (blue curve). It should be mentioned that the high liquefaction resistance exhibited by the laminated samples subjected to CTX loading is not only attributed to the high clay lamination content, but also to the type of loading.

For comparison, the plot on Fig. 5 also includes experimentally obtained liquefaction resistance curves for a typical clean sand (i.e. Nevada sand) for relative densities, D_r , between 40% and 60% [23], and for a soft clay from Adapazari, Turkey [12]. It is worth mentioning that the estimated relative density of the uniform sand samples varies between 45% and 55% falling within the range of liquefaction resistance exhibited by Nevada sand with similar values of relative density. The estimation of the relative density of uniform sand samples was primarily based on interpreted CPT data obtained in areas where the sand layers were thick enough to allow for full development of the tip resistance (i.e. layers with thicknesses of more than about 0.3 m).

3. Numerical investigation of liquefaction resistance of laminated soils

In addition to advanced cyclic tests, numerical evaluations at a

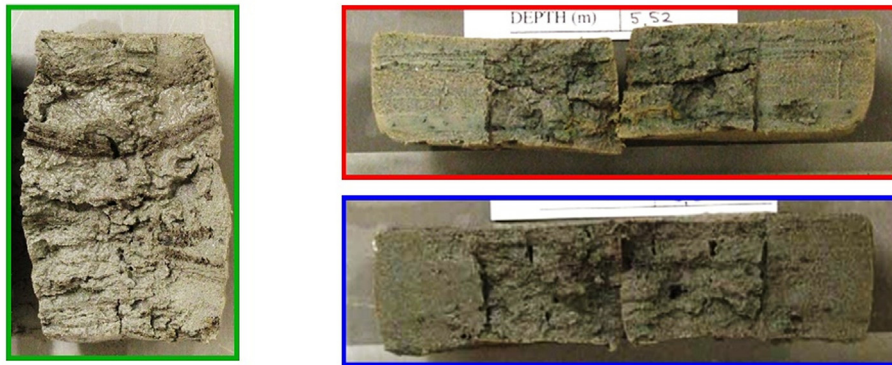
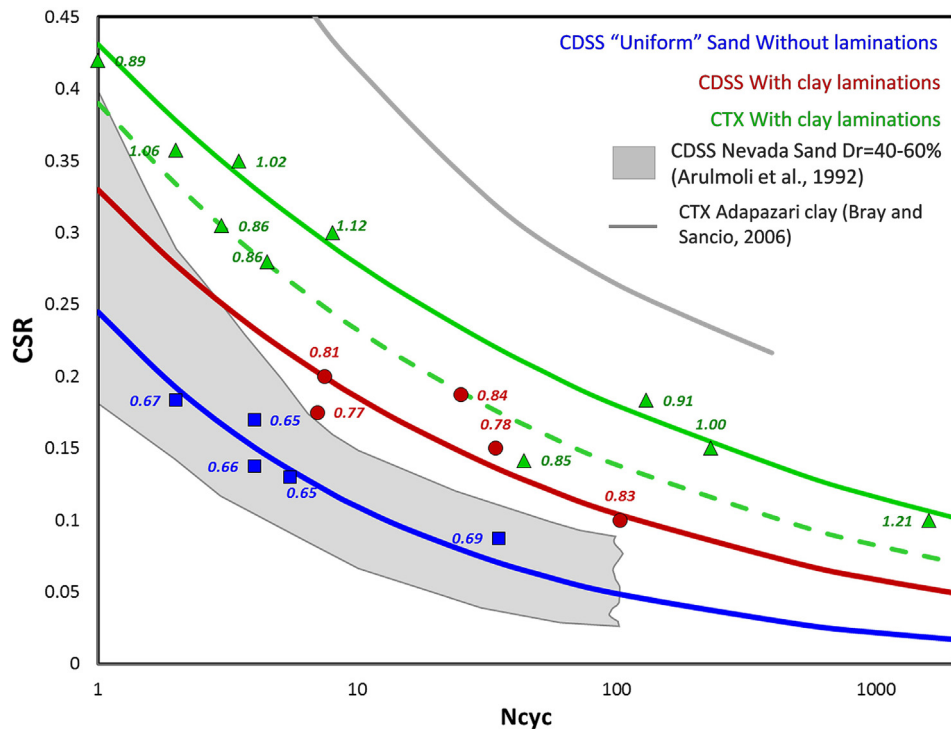


Fig. 5. Liquefaction resistance curves (blue, red and green) obtained from laboratory cyclic testing without static bias. The characteristic sample photos below the graph correspond to each curve. The initial void ratio is labeled next to the marks corresponding to each test. The grey area and curve correspond to Nevada sand for a range of relative density, D_r , between 40% and 60% [23], and to a soft clay from Adapazari, Turkey [12], respectively.

sample scale were performed with FLAC2D [24] using advanced constitutive models to simulate the sand behavior while explicitly modeling the clay laminations. After calibration and validation of numerical simulations against laboratory tests in terms of shear strain accumulation and excess pore pressure development versus the number of loading cycles, parametric numerical investigation was conducted to shed light on the effect of the clay lamination percentage on the liquefaction resistance and post-liquefaction deformation.

3.1. Constitutive model calibration for uniform sand samples

The first step of the numerical investigation involved the simulation of the uniform sand samples exhibiting the lowest liquefaction resistance. To this end, UBCSAND [25] and PM4Sand [26,27] constitutive models were calibrated in order to capture liquefaction triggering and shear strain accumulation behavior for both level (no-bias) and sloping ground (bias) conditions following methodologies described by Giannakou et al. [28]. It should be noted that a single set of parameters for each constitutive model was used for the calibration process, aiming to capture the liquefaction triggering curve drawn with a blue line in

Fig. 5, by assuming a cohesionless soil with relative density, D_r , equal to about 50%. Subsequently, these two sets of parameters, one for each constitutive model, were used to model the sand laminations throughout this study.

Fig. 6 depicts the liquefaction resistance curves obtained by the calibrated constitutive models compared to those interpreted from laboratory test results. Fig. 7 presents shear stress-strain loops and stress paths from CDSS tests on a uniform sand sample ($CSR = 0.183$) with no initial static bias, together with stress-strain loops and stress paths derived from the calibrated UBCSAND and PM4Sand models. In the same manner, Fig. 8 demonstrates shear stress-strain loops and stress paths obtained from both experimental and numerical CDSS tests on a uniform sand sample with initial static bias equal to 0.2. The reasonable comparison between observed and simulated behavior suggests that the calibrated constitutive models can adequately simulate the cyclic behavior of the sand both in terms of liquefaction triggering and in terms of post-liquefaction shear strain accumulation

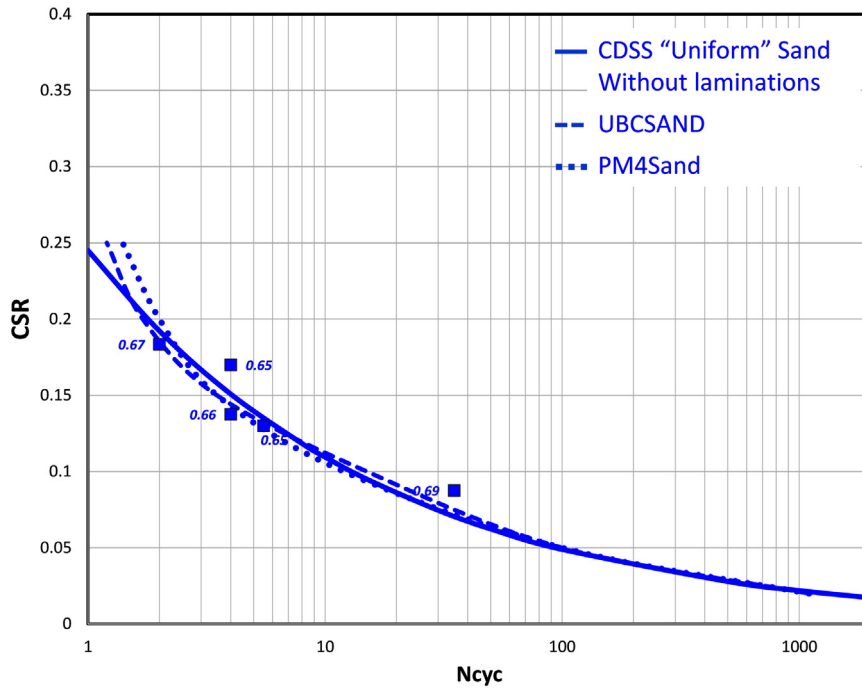


Fig. 6. Comparison between experimental and numerical liquefaction resistance curves for uniform sand samples subjected to CDSS loading (without static bias).

3.2. Simulation of laminated samples under cyclic direct simple shear loading

Aiming to reproduce numerically an undrained CDSS test without static bias on a laminated sample ($CSR = 0.2$ on red curve of Fig. 5), a composite numerical model was built including both sand and clay laminations. Using a sample photo (Fig. 9a) and X-ray tomography (Fig. 3), two 0.6-cm-thick clay laminations were identified within the sample, corresponding to a clay lamination percentage (herein noted as

CLP) equal to 40%. The composite numerical model of the sample, constructed in FLAC2D [24] and shown in Fig. 9b, consists of a 3 cm-high grid containing 10 elements, each corresponding to either sand or clay material. The sand laminations were modeled with the UBCSAND and PM4Sand models calibrated for uniform sand samples (Fig. 6), as described in Section 3.1. The clay laminations were modeled as Mohr-Coulomb material with an undrained shear strength, S_u , equal to 40 kPa which is a representative value for the vertical effective stress range of the tests. Estimates of undrained shear strength for clay laminations

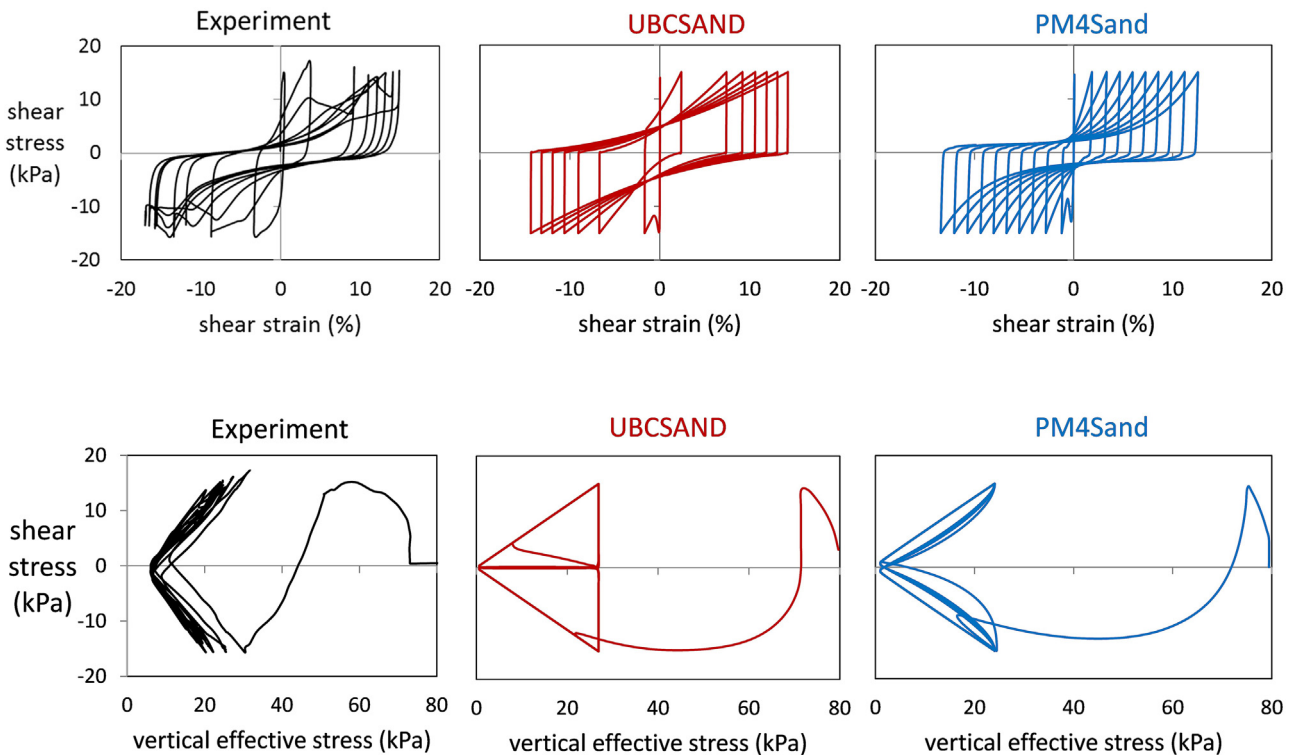


Fig. 7. Comparison between experimental and numerical results on a uniform sand sample ($CSR = 0.183$) subjected to CDSS loading with no initial static bias.

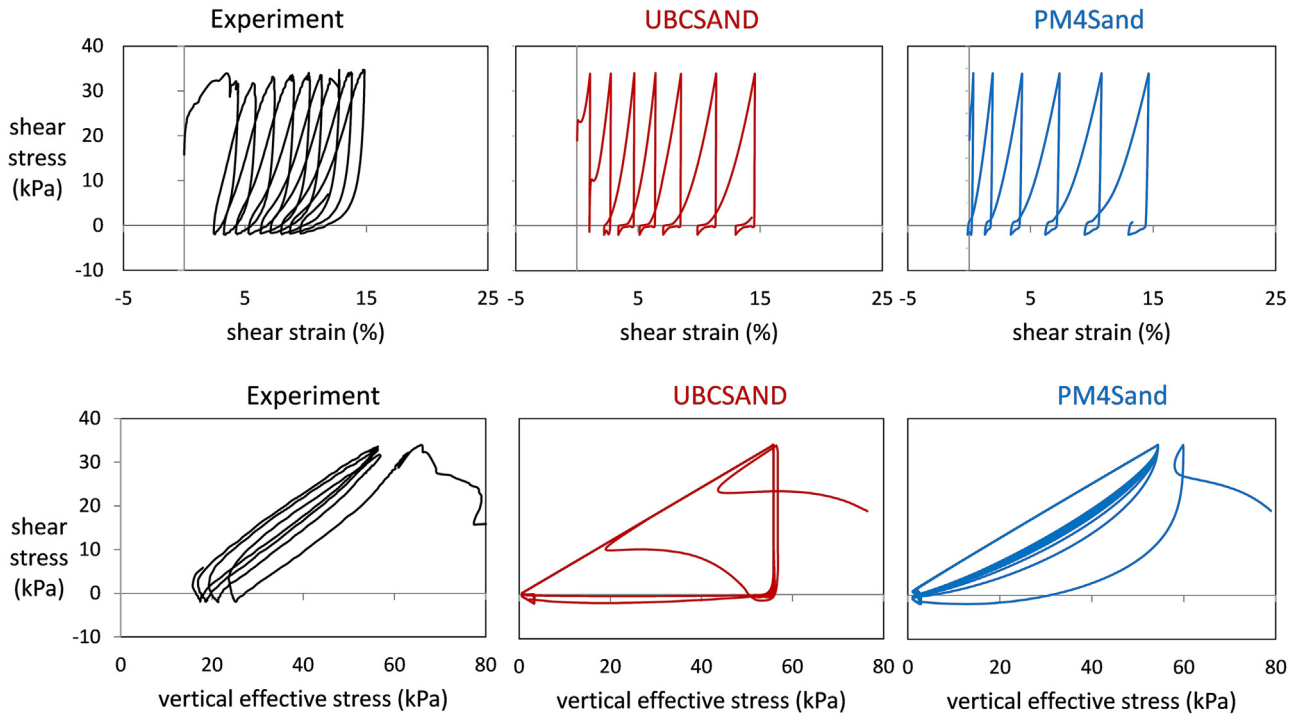


Fig. 8. Comparison between experimental and numerical results on a uniform sand sample subjected to CDSS loading with initial static bias equal to 0.2.

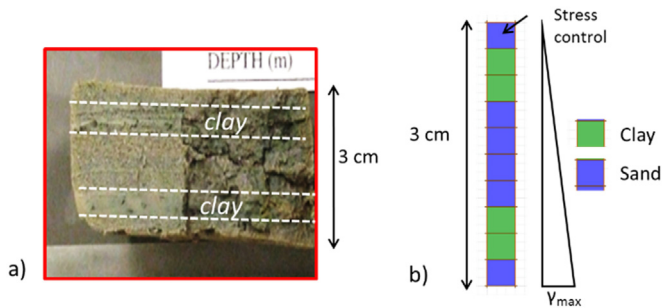


Fig. 9. a) Photo of a laminated sample subjected to CDSS testing, b) Composite numerical model of the laminated sample.

were interpreted from CPT data and UU tests in thicker clay layers encountered below the laminated deposits where the tip resistance is not influenced by the presence of sand laminations and where it was possible to retrieve samples of sufficient height for UU tests. Atterberg limit measurements on clay samples indicated Plasticity Index values ranging between 20% and 45% and liquid limits of more than 50%.

A comparison between numerical simulations and experimental results, illustrated in Fig. 10, indicates that an accurate numerical simulation in terms of geometry and calibrated effective stress parameters can reproduce the experimental response of laminated deposits in terms of liquefaction resistance and post-liquefaction deformations. Subjecting the composite numerical model of Fig. 9b to various CSR levels, the liquefaction resistance curve for CLP = 40% was developed and plotted on Fig. 11.

3.3. Effect of clay lamination percentage on liquefaction resistance

After validating the composite numerical model against laboratory data in Section 3.2, the same exercise was repeated using composite numerical models with various clay lamination percentages (CLPs). Fig. 12 presents liquefaction resistance curves obtained numerically for CLPs ranging from 10% to 60% (grey lines) plotted together with the laboratory data. The trend that was observed in the laboratory is also

reflected in the numerical evaluations: As the clay lamination percentage increases, the liquefaction resistance of the laminated samples increases as well. In particular, numerical simulations show that even the presence of a small amount of clay laminations in the sample (i.e. CLP = 10%) results in a significant increase of cyclic resistance compared to the uniform sand sample. It is worth noting that parametric numerical analyses with different configurations of sand-clay laminations for a given CLP indicate that the distribution of the clay laminations within the sample has negligible impact on the liquefaction resistance.

3.4. Simulations of laminated samples subjected to cyclic plane strain compression loading

A composite numerical model was built to reproduce an undrained CTX test on a laminated sample using PM4Sand model for the sand laminations. Due to limitations regarding the formulation and implementation of PM4Sand in FLAC2D [24], being currently restricted to plane strain conditions, the composite numerical model was subjected to cyclic plane strain compression instead of cyclic triaxial compression.

Before proceeding to the numerical simulation of a real laminated sample tested in the laboratory, simulations were performed using idealized numerical models in order to identify the deformation mechanisms due to plane strain compression such as the shear band formation in uniform sand material. Two idealized models were built consisting of: i) uniform sand and ii) alternating laminations of sand and clay materials. The sand layers were assigned similar properties to the uniform sand sample (Section 3.1), while the clay layers were modeled as Mohr-Coulomb material with an undrained shear strength of 40 kPa. The numerical model was 14 cm high and 7 cm wide forming a dense grid with an element size of 7×7 mm, in order to be able to capture potential (grid-sensitive) strain localization. Lateral and vertical stresses were applied at the external boundaries of the model, while the base of the model was fixed. Subsequently, the two idealized models were subjected to both monotonic and cyclic plane strain compression by applying vertical velocity at the top of the model.

Fig. 13 illustrates the two idealized models together with the

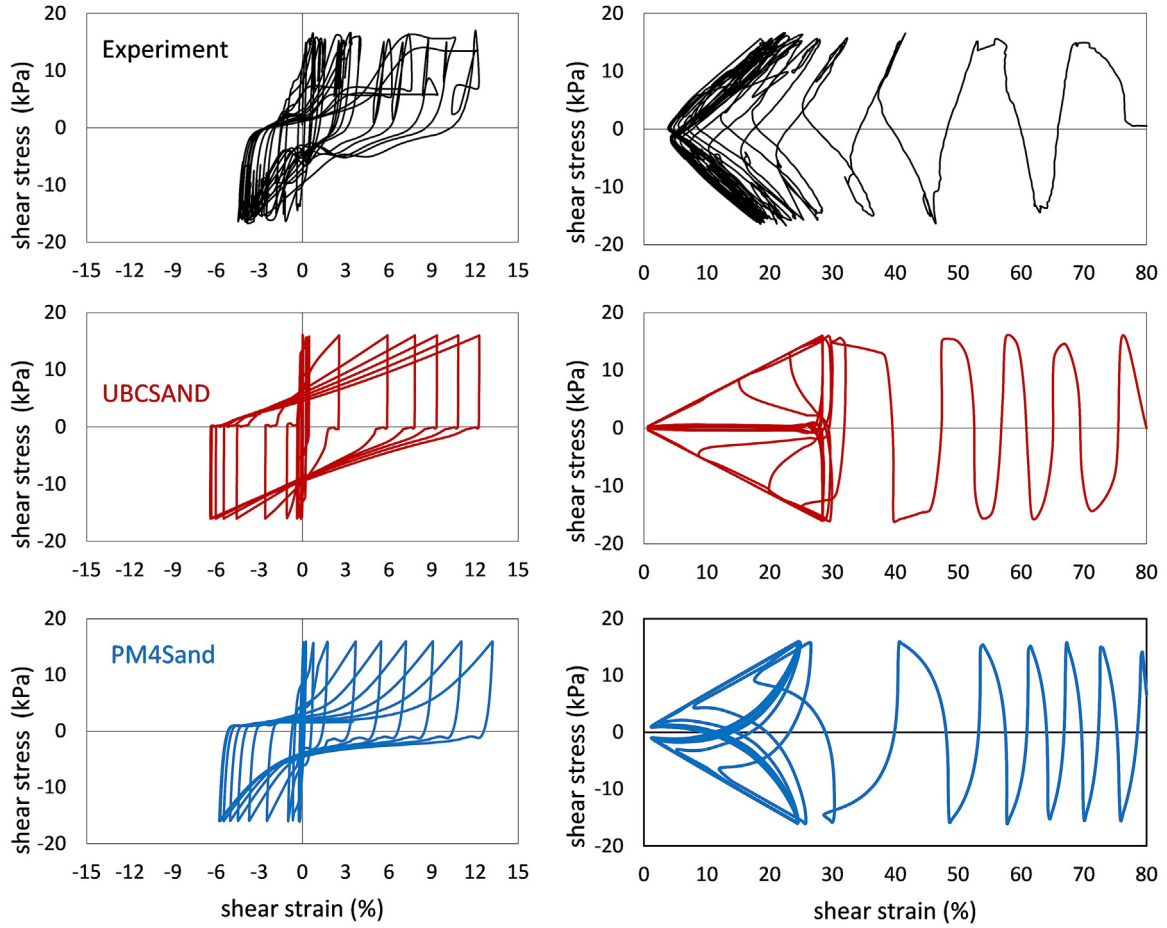


Fig. 10. Comparison between experimental and numerical results of a laminated sample (-CSR=0.2) subjected to cyclic simple shear loading.

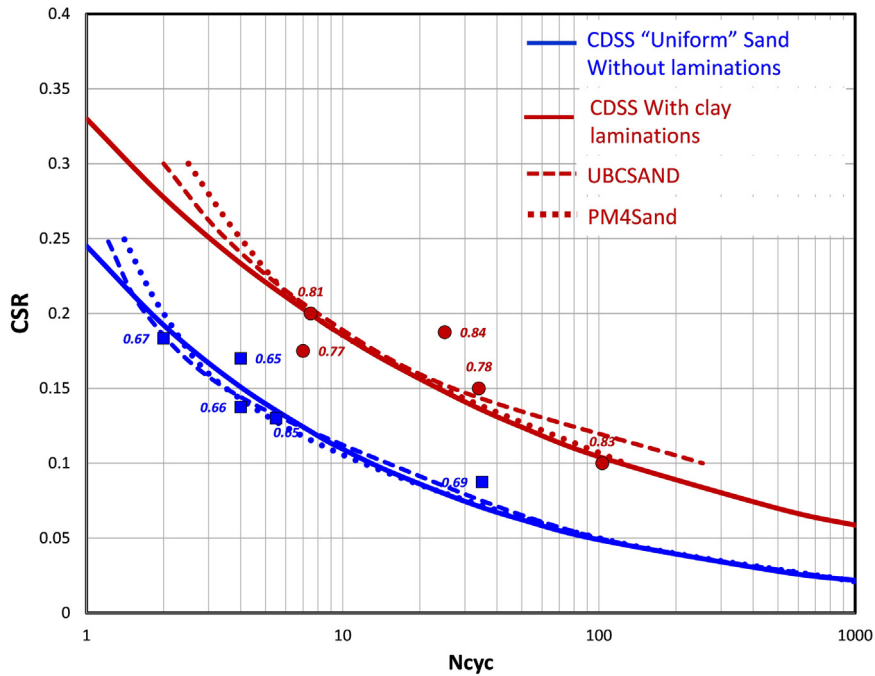


Fig. 11. Liquefaction resistance curves obtained from the composite numerical model (Fig. 9b) with CLP = 40% subjected to CDSS loading are compared with experimental data on laminated samples (red symbols).

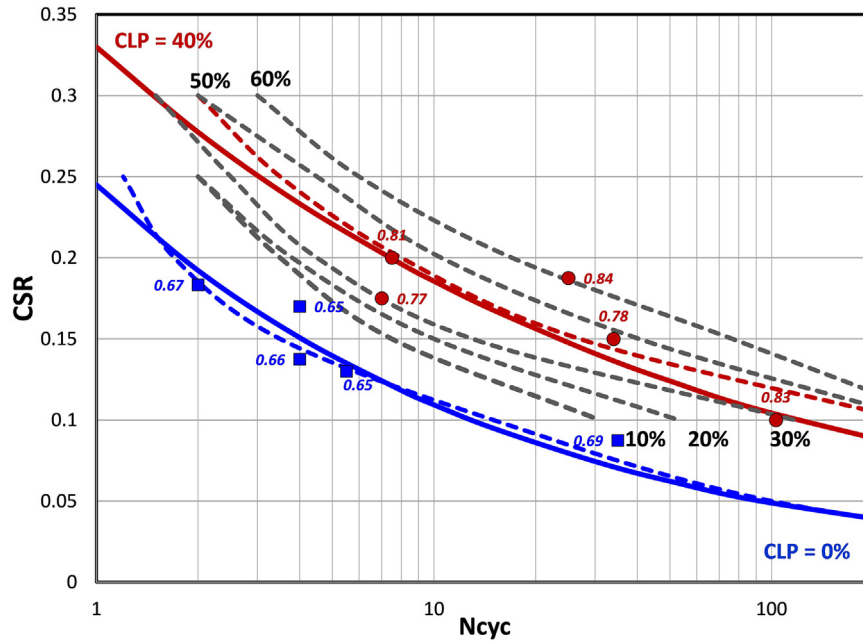


Fig. 12. Liquefaction resistance curves (dashed grey lines) for various clay lamination percentages (CLPs) obtained from composite numerical models subjected to CDSS loading are plotted together with experimental data (blue and red symbols, corresponding to uniform and laminated samples, respectively).

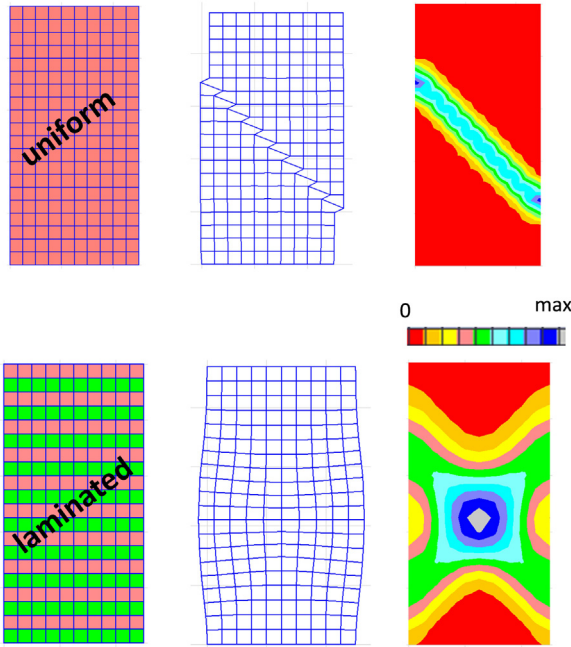


Fig. 13. Deformed meshes and contours of shear strain for idealized models consisting of uniform sand (top) and laminated soil with alternating layers of sand and clay (bottom) subjected to monotonic plane strain compression.

deformed meshes and the shear strain contours obtained from monotonic plane strain compressional loading. The deformation patterns obtained from the two models differ. In case of the uniform sand model, a localized shear band is developed, as expected, while in case of the laminated model, the presence of the clay laminations causes distributed shearing and an overall bulging deformation pattern.

Fig. 14 depicts the results obtained from the two idealized models subjected to cyclic plane strain compression in terms of: a) contours of the number of cycles required to develop 1.5% local axial strain and b) the liquefaction resistance curves with a criterion of 1.5% total axial strain. The numerical results indicate that the presence of the clay

laminations tends to increase the liquefaction resistance and inhibit strain localization.

As a second step, numerical simulations of actual laminated samples were performed. Fig. 15a shows the X-ray image and the composite numerical model of a laminated sample that was subjected to CTX testing ($CSR = 0.28$ on green dashed curve of Fig. 5). The discretization is very dense with an element size of 2×2 mm, allowing for modeling of extremely thin clay laminations.

The deformed shape of the composite numerical model is compared with the cyclic triaxial sample on Fig. 15b, exhibiting similar characteristics. Fig. 16 depicts the development of axial strains versus cycles of loading. The total axial strain from the simulation was estimated by tracking the change of the sample height and dividing it by its initial height, similar to the measurements made in the laboratory. Both experiment and simulation suggest triggering (1.5% axial strain) at about 4–4.5 cycles. The cyclic responses are also compared in terms of stress-strain plots, and stress paths. In the numerical simulation, the deviatoric stress, q , was measured at the middle top element of the grid, in the sand material.

Despite the differences between the simulation and the experiment, attributed to the idealization in the configuration of the clay laminations, the different type of loading (plane strain versus triaxial compression) and the simplified modeling of clay as a Mohr-Coulomb material, the overall reasonable comparison provides a level of confidence in the use of the calibration process and the available numerical tools. Moreover, a noteworthy observation is that within highly laminated materials, the presence of the clay laminations tends to limit the development of strain localization.

3.5. Evaluation of conversion factor from cyclic triaxial to cyclic simple shear loading on laminated samples

Although CDSS testing provides loading conditions which are more representative of an earthquake, the height limitations of the specimen (i.e. 3 cm) in combination with the nature of the laminated deposits (i.e. clay lamination thickness on the order of 1–2 cm) necessitated CTX testing which allows for taller specimens. Therefore, laminated samples were primarily tested under CTX loading conditions while a limited number was subjected to CDSS testing.

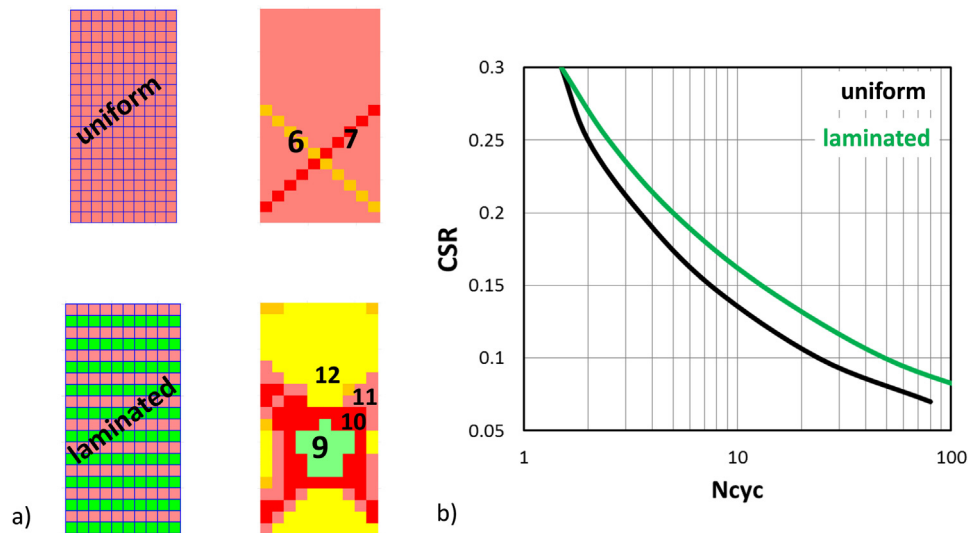


Fig. 14. a) Contours of number of cycles required to cause 1.5% local axial strain under cyclic plane strain compression loading. b) Liquefaction triggering curves with a criterion of 1.5% total axial strain.

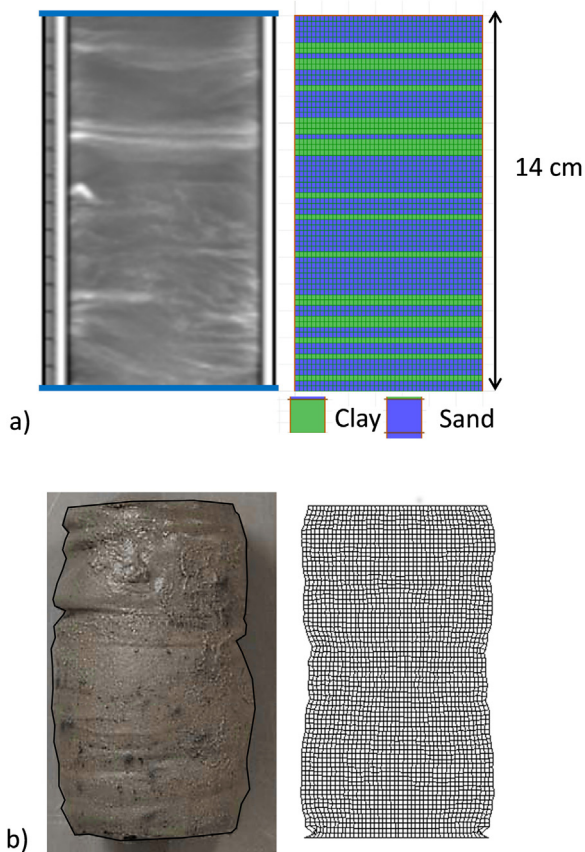


Fig. 15. a) X-ray section and composite numerical model of a laminated sample subjected to CTX loading. b) The deformed sample and mesh at the end of the loading.

In order to correlate the two cyclic testing types, a conversion factor ranging from 0.6 to 0.7 (applied to CSR obtained from CTX tests) is recommended by various researchers based on data for clean sands [3,29–34]. The recommended conversion factor for clean sands mainly depends on the value of the coefficient of earth pressure, K_0 , at the consolidation stage. When studying the liquefaction susceptibility of a normally consolidated fine-grained soil deposit after the 1989 Loma

Prieta earthquake, Boulanger et al. [35] used a conversion factor of 0.7. Donahue et al. [22] used a conversion factor of 0.84 based on results from CDSS and CTX tests on fine-grained samples reconstituted with the Slurry Deposition Method and tested at an effective confining pressure of 50 kPa. Sancio [36] found a conversion factor of 0.85 when testing shallow, fine-grained soils from Adapazari with a plasticity index, PI, less than 12, at a mean effective stress equal to 100 kPa.

In an attempt to evaluate the conversion factor between CTX and CDSS tests on laminated deposits, numerical simulations were performed. Initially, numerical simulations were performed to estimate the conversion factor between CTX and CDSS tests on a uniform sand sample. PM4Sand constitutive model was used to model the cyclic behavior of a uniform sand sample that was calibrated to the interpreted CDSS lab results on uniform (non-laminated) sands samples (see Fig. 6). The uniform sand model was subjected to both cyclic direct simple shear (CDSS) and plane strain compressional (CPS) loading; the latter was considered to approximate cyclic triaxial loading (CTX). K_0 values equal to 0.5 and 1 were assumed for CDSS and CPS loading, respectively.

The resulting conversion factors range between 0.64 and 0.72 for a uniform sand sample, which is in agreement with the range of values suggested in literature for clean sands. Fig. 17a depicts the liquefaction triggering results from numerical simulations under CDSS and CPS loading using a uniform sand model, as well as the converted CPS curve to equivalent CDSS one using an average conversion factor equal to 0.67.

As a second step, the same procedure was followed using the composite (laminated) numerical model used in Section 3.4 (Fig. 15). The resulting conversion factors range between 0.78 and 0.83 for the laminated sample, which are higher than the conversion factors for uniform sand deposits, but in line with the experimental findings on fine-grained samples discussed above. Fig. 17b depicts liquefaction resistance curves from numerical simulations under CDSS and CPS loading using a composite model, as well as the converted CPS curve to equivalent CDSS one using an average factor equal to 0.8.

Based on the numerical evaluations, a conversion factor of 0.8 was applied on the cyclic stress ratios obtained from CTX testing on laminated samples in the laboratory, in order to obtain equivalent CDSS cyclic stress ratios. The experimental results obtained from CDSS tests and converted CTX tests are plotted on Fig. 18 together with the liquefaction resistance curves for different clay lamination percentages (CLPs) predicted numerically. It is observed that the converted CTX experimental liquefaction resistance curves (solid and dashed green

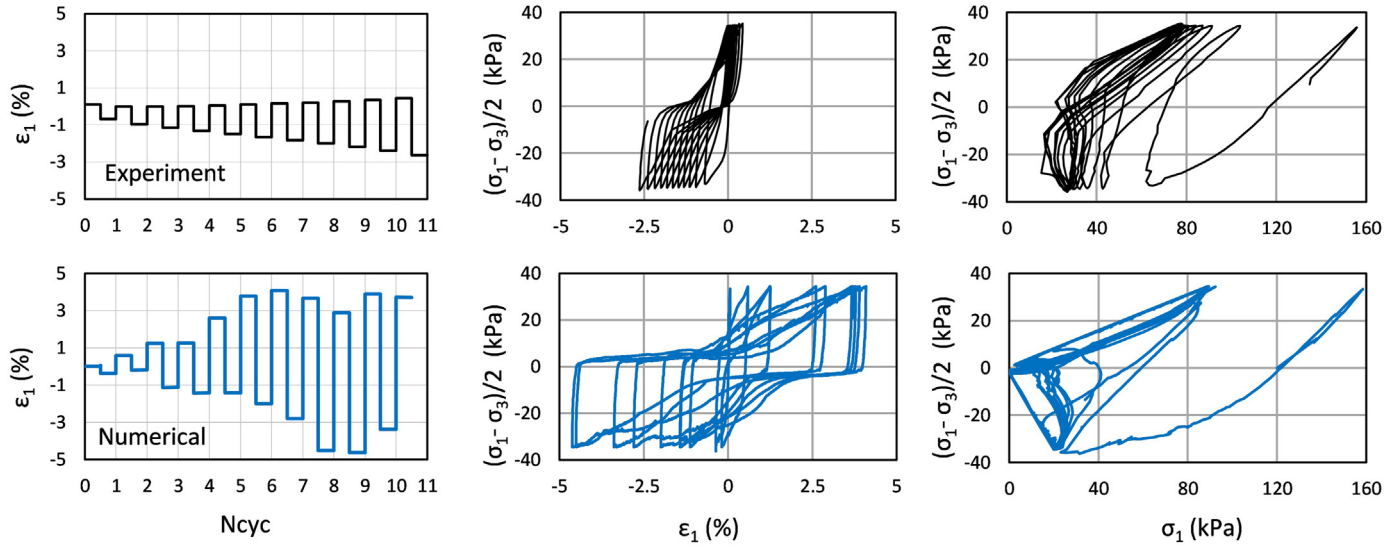


Fig. 16. Comparison between numerical (using PM4Sand model) and experimental results obtained from cyclic plane strain compression and triaxial compression loading, respectively, on a laminated sample with CSR = 0.28.

lines) are close to the numerically estimated triggering curves corresponding to CLPs between 40% and 60%.

4. Numerical investigation of post-liquefaction deformation of laminated deposits

The thin nature of the sand and clay laminations currently renders their explicit modeling in 2D numerical models impracticable due to the large computational time required. In an attempt to overcome this limitation, one option would be to calibrate the sand constitutive models to the triggering curves interpreted from the cyclic tests on laminated samples (i.e. red curve on Fig. 18). In this case, each element would simulate the equivalent macroscopic behavior of the laminated material rather than the behavior of the sand layers and the clay laminations separately. However, the following question arises: would this macroscopic treatment be equivalent to the more realistic explicit modeling of sand and clay laminations under earthquake loading especially in terms of co-seismic and post-liquefaction deformations, such as stain localization at the sand/clay interfaces due to stiffness contrast and void redistribution effects?

To address this issue, numerical simulations were performed at a system level, using a 1D soil column, under earthquake loading. The numerical investigation focuses on the response of laminated soils in terms of liquefaction triggering, post-liquefaction deformation accumulation under sloping ground conditions, and void redistribution effects.

4.1. Post-liquefaction shear-strain accumulation

One dimensional nonlinear effective stress site response analyses were performed to investigate the dynamic response of thinly laminated deposits under groundwater flow and sloping ground conditions. A finite difference mesh of a 1D soil column was created using a fine discretization of 20-cm-thick elements for the laminated intertidal deposits whose total thickness is 5 m (Fig. 19).

Sand laminations were modeled with PM4Sand and UBCSAND, while clay laminations were modeled with a Mohr-Coulomb failure criterion in combination with a nonlinear stress-strain behavior using the Itasca S3 hysteretic model [24]. In order to model static bias conditions in 1D site response, the 1D column was inclined simulating an

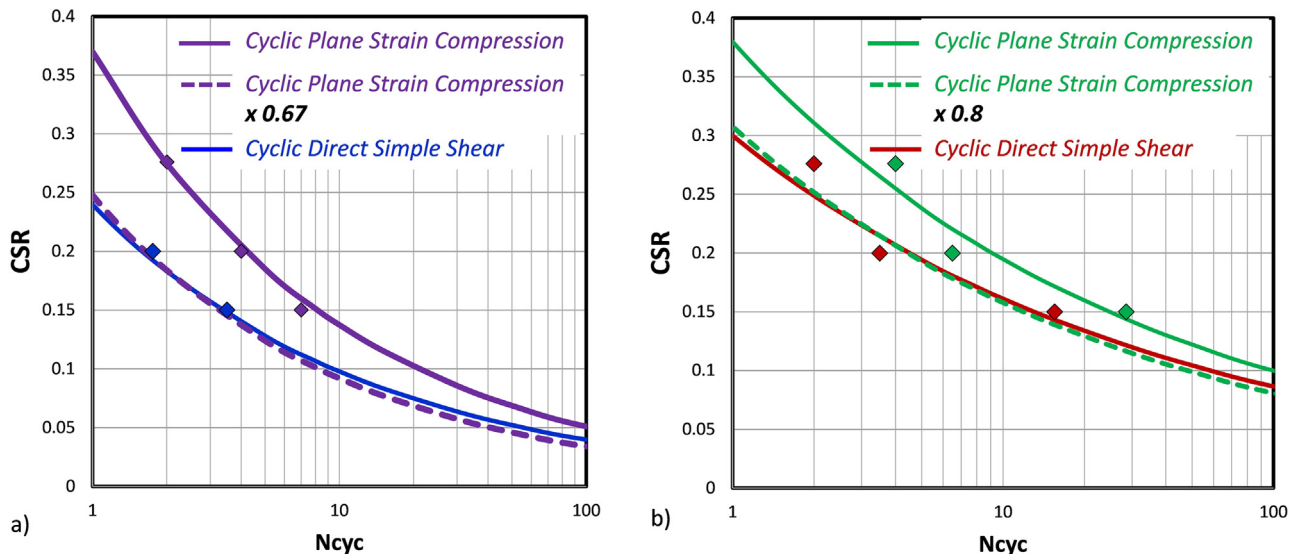


Fig. 17. Liquefaction resistance curves obtained from numerical simulations: (a) on uniform sand and (b) composite (laminated) models.

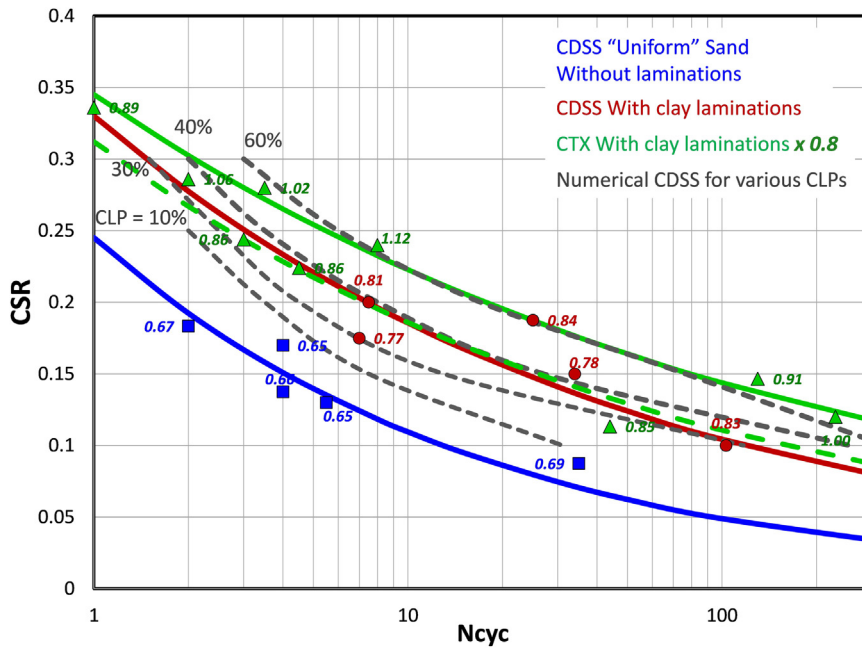


Fig. 18. Experimental and numerical liquefaction resistance curves for laminated deposits with different clay lamination percentages (CLPs).

infinite slope with a static shear stress ratio equal to 0.1. An input seismic motion with $PGA = 0.23\text{ g}$ was applied to the base of the model.

In order to compare the dynamic behavior resulting from the use of uniform macroscopic properties with the one obtained from explicit modeling of the laminations, three different configurations were selected (illustrated in Fig. 19):

- Case A. All elements were modeled as sand material without clay laminations (blue curve)
- Case B. Elements were modeled with uniform macroscopic properties for laminated deposits equivalent to the red curve

corresponding to a CLP equal to 40%.

- Case C. The sand (blue curve) and clay laminations of the intertidal deposits were explicitly modeled with a CLP equal to 40%.

Fig. 20 presents the results for the three cases in terms of maximum excess pore pressure ratio and residual lateral displacements versus depth. In Case A, liquefaction is triggered resulting in a maximum excess pore pressure ratio of 1 throughout the sand layer and a ground surface lateral displacement in the order of 0.65 m. In Case B where the tidal deposits comprise of sand with higher CRR, corresponding to laminated material, liquefaction is only triggered near the base of the layer for both constitutive models. Residual lateral displacement is on

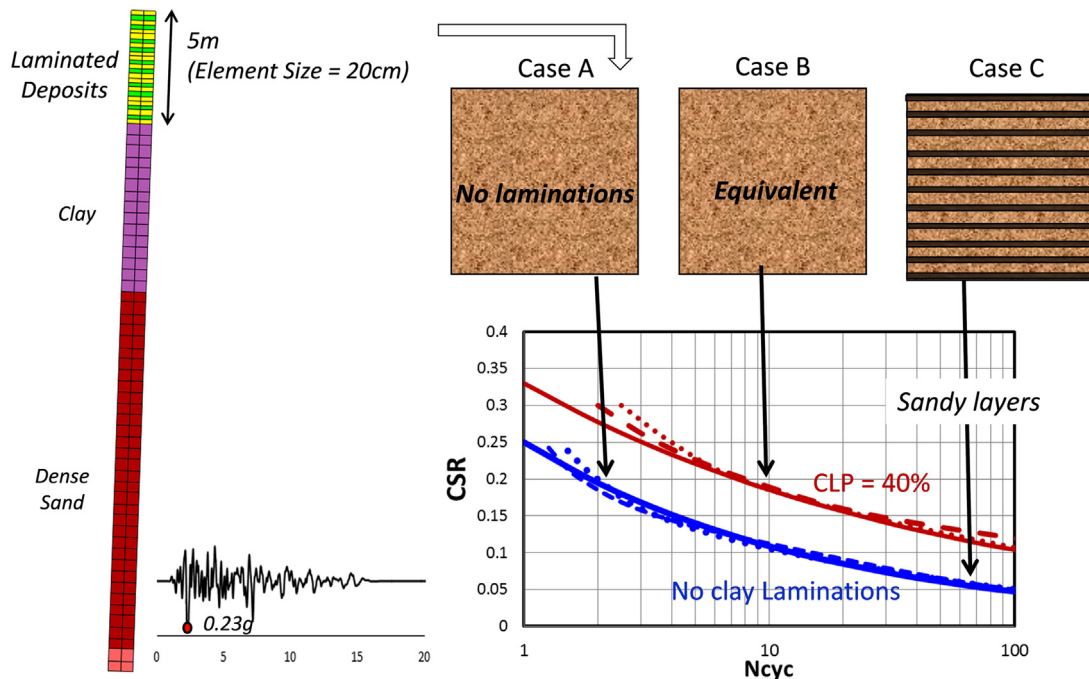


Fig. 19. 1D numerical model and three different configurations of the tidal deposits which are modeled as: A) uniform sand (blue curve), B) uniform sand (red curve) and C) laminated deposits with alternating laminations of sand (blue curve) and clay.

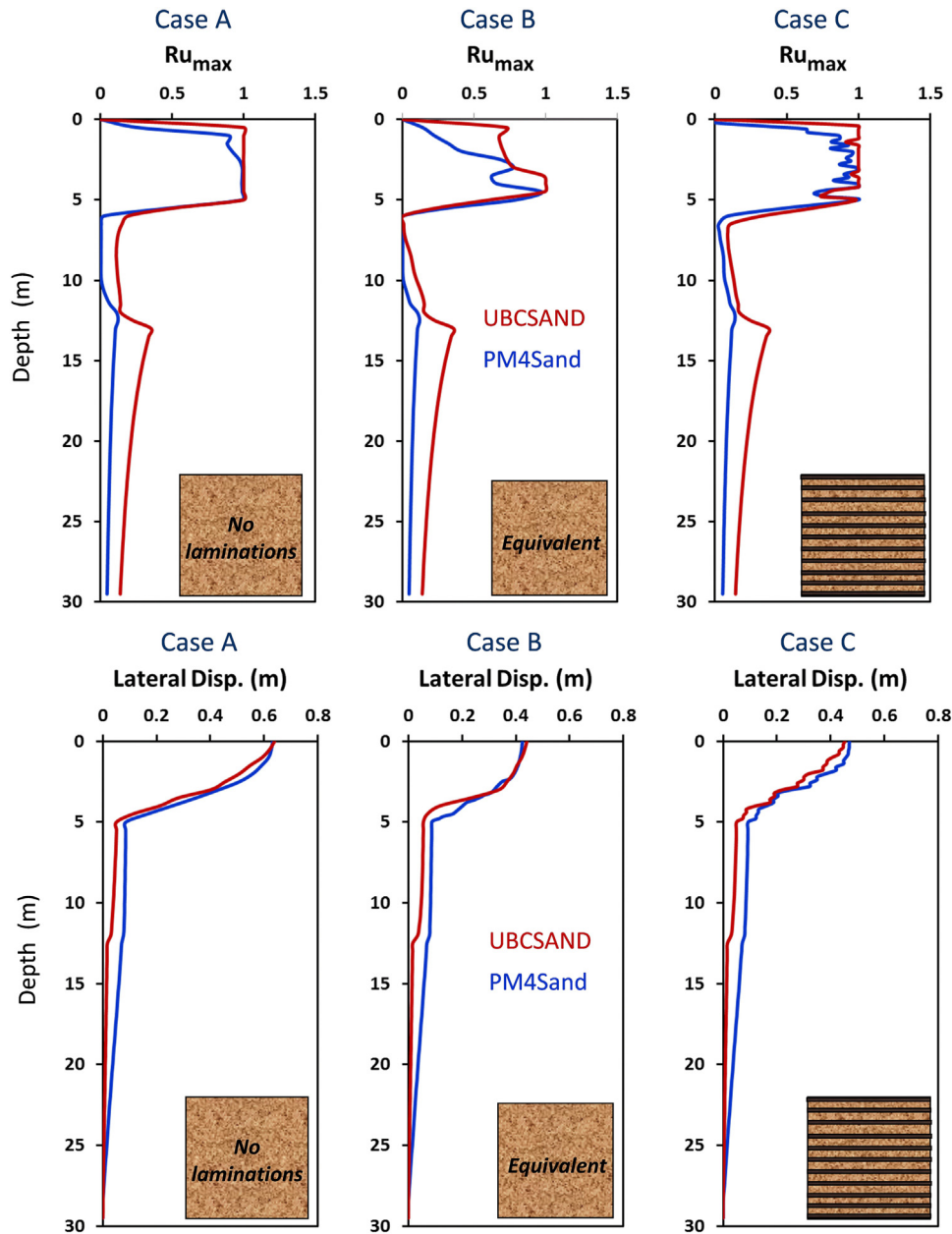


Fig. 20. Maximum excess pore pressure ratio (top) and residual lateral displacement (bottom) versus depth for the three cases presented in Fig. 18.

the order of 0.43–0.44 m corresponding to a ~30% reduction relative to Case A. In Case C, where the sand and clay laminations are modeled explicitly, residual lateral displacement is in the order of 0.45–0.47 cm, indicating that the presence of clay laminations impedes the development of large deformations due to liquefaction. Perhaps most importantly, the system dynamic response in Case B, where equivalent macroscopic properties are used to model the cyclic resistance of laminated deposits, is quite similar to the system dynamic response of Case C, where the sand and clay laminations are modeled explicitly. The same exercise was repeated for CLPs equal to 20% and 60% and similar conclusions were deduced, providing confidence that equivalent macroscopic properties can be used for more complex 2D numerical analyses (with similar soil conditions and shaking levels) to model the behavior of laminated deposits, after appropriate calibration.

4.2. Void redistribution effects

In sand and clay laminated deposits, the presence of clay

laminations causes permeability contrasts that tend to inhibit the dissipation of cyclic-induced pore pressures developed within the sand laminations, theoretically resulting in void redistribution and potential strain localization [37–41]. Parametric numerical investigations were performed to evaluate the potential for void redistribution with respect to the thickness of the sand laminations. Effective stress nonlinear response analyses were performed for a 1D profile using a very fine discretization of 5-cm-thick elements to model the laminated deposits. In order to study void redistribution effects, the input ground motion was scaled up to ensure that the sand laminations liquefied in all cases analyzed. Additionally, relatively high permeability was used for the sand layers so that void redistribution effects could develop at the end of shaking. Fig. 21 summarizes the cases considered in these sensitivity analyses and presents the results of the parametric investigation in terms of relative density at the end of shaking and maximum excess pore pressure ratios versus depth. For the estimation of relative density during and after shaking, minimum and maximum void ratios were assumed equal to 0.5 and 0.8, respectively. The following observations

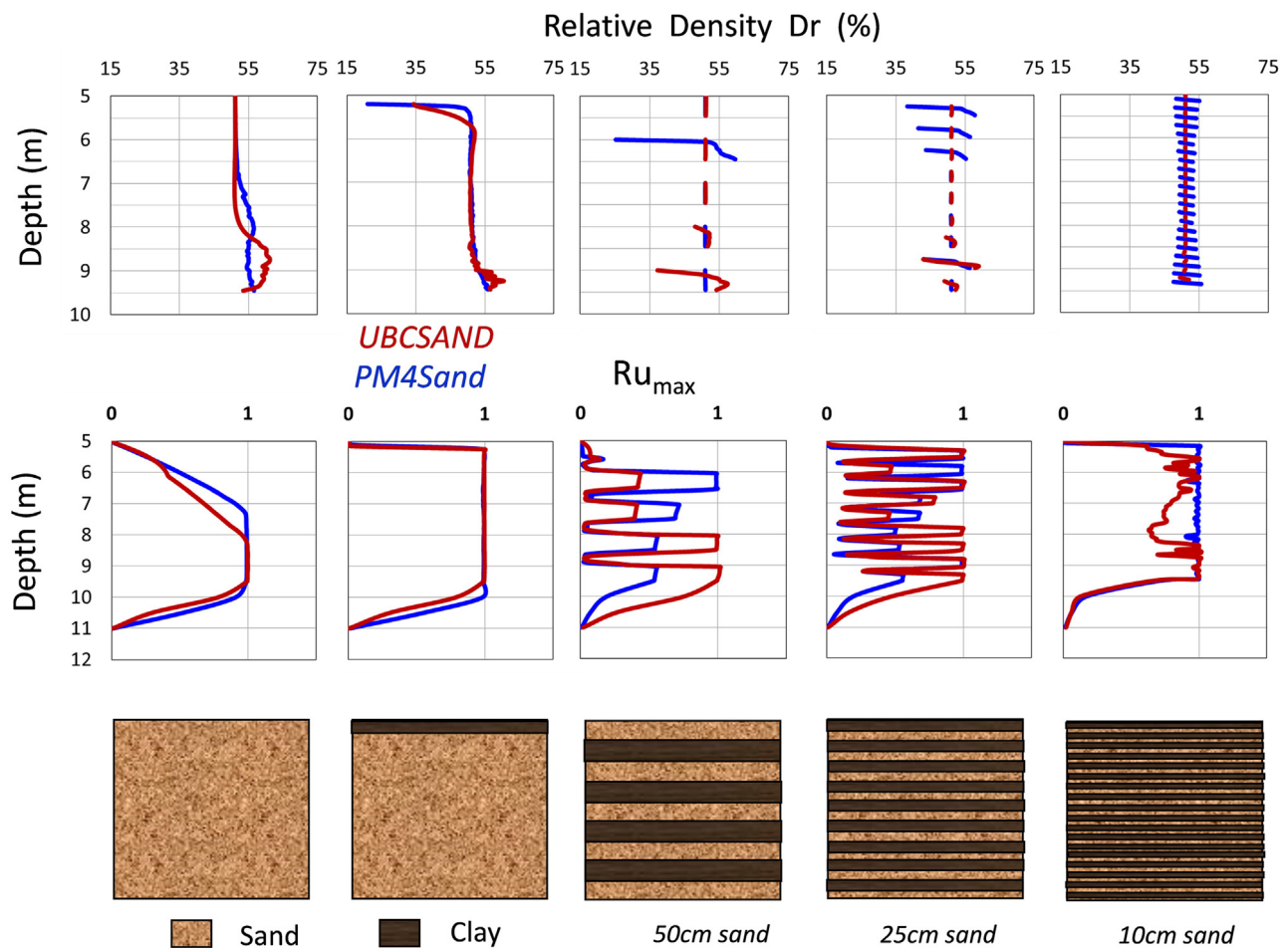


Fig. 21. Variation of relative density within sand layers due to void redistribution effects.

are noteworthy:

- In the first case (first graph from left on Fig. 21) where a uniform sand layer is modeled with no clay laminations, excess pore pressures migrate freely from the bottom part towards the phreatic surface resulting in densification of the bottom part of the layer. No significant void redistribution effects that would lead to shear strain localization are observed in this case.
- When a clay lamination is present at the top of the sand layer, free dissipation close to the surface is inhibited resulting in accumulation of excess pore water pressures close to the sand/clay interface and subsequent loosening of the sand layer below the clay lamination. Densification is still observed at the bottom part of the layer. This is depicted on the second graph from the left on Fig. 21 where the relative density of the sand layer below the clay lamination reduces to 15–35% whereas it increases close to the bottom of the layer. Evidently, void distribution effects are significant in this case causing shear strain localization at the sand/clay interface.
- The effect of void redistribution, which is indicated here through the decrease in relative density (loosening), diminishes as the thickness of the sand laminations decreases. This is observed by comparing the 2nd, 3rd, 4th and 5th graph on Fig. 21, where it is shown that relative density at the end of shaking reduces to 35%, 49%, 76% and 95% of its initial value for a 4.5-m-, 0.5-m-, 0.25-m- and 0.10-m-thick sand layer, respectively.

The results described above illustrate the mitigating effect of thin clay layers within the laminated deposits on the potential for void redistribution. It should be mentioned that the effect of void

redistribution not only diminishes as the thickness of the sand lamination decreases – a finding consistent with experimental and numerical studies by Kulasingam et al. [42], Sento et al. [43] and Malvick et al. [44] – but also as the permeability contrast between the laminations decreases.

5. Conclusions

Advanced cyclic laboratory tests on both uniform sand samples and laminated (sand/clay) ones and subsequent numerical reproduction of these tests provided evidence that the presence of clay laminations tends to increase the liquefaction resistance of the overall deposit. Similarly, parametric numerical analyses on laminated samples subjected to cyclic direct simple shear (CDSS) loading revealed a systematic trend: laminated deposits become more resistant to liquefaction, as the clay lamination percentage increases. In addition, numerical investigations of the behavior of laminated samples under cyclic plane strain compression loading (approximation of cyclic triaxial loading CTX), indicated that clay laminations tend to hinder the development of strain localization leading to distributed strains and a different type of failure mode than the one observed in uniform sand samples.

Moreover, numerical simulations of laminated samples under cyclic plane strain compression loading were used to develop estimates of a conversion factor between CTX and CDSS test results for laminated samples. Based on these evaluations, a factor of 0.8 was used to convert the CSR from CTX tests to equivalent CSR of CDSS tests.

Last, 1D site response numerical analyses, involving explicit modeling of the sand/clay laminations, showed that: i) laminated soils can be modeled as uniform sand materials using advanced constitutive

models calibrated to the composite (macroscopic) behavior measured in laboratory tests on laminated samples and ii) void redistribution effects, often considered a source of strain localization tend to be significantly reduced as the thickness of sand lamination decreases, or as the percentage of clay laminations increases.

The findings of this study focus on natural intertidal laminated soil deposits encountered at a specific site. However, these soils are frequently encountered in many parts of the world, and their earthquake response is often estimated using in situ measurements (CPT and SPT) and established (conventional) simplified methods that have been developed for sand materials. Given the interlayered nature of these deposits, and the dimensions of standardized in situ tests, the estimated earthquake responses are overly pessimistic and can sometimes lead to the implementation of unnecessary or excessive mitigations. This study has attempted to shed light on the basic trends in the behavior of laminated soil deposits under cyclic loading, based on both experimental and numerical evidence. Moreover, it has raised the need for further systematic experimental research both on natural samples and reconstituted samples in the lab with well-defined properties in order to identify the main parameters that affect the response and to quantify those parameters at specific sites using in situ and laboratory tests.

Acknowledgements

The experimental and numerical work described in this paper was funded by Nederlandse Aardolie Maatschappij B.V. (1016-0459-000) (NAM). Edith van Dijk from the NAM team must be credited for having the courage and vision to go beyond conventional engineering procedures to use the most advanced tools available to address this difficult problem. Professors Steven Kramer and Russell Green from the Peer Review Panel provided valuable guidance and oversight to this work. David Trowbridge and Mike Rattley from Fugro oversaw the advanced experimental testing work which was conducted in Fugro's Wallingford lab in the UK.

References

- [1] Youd TL, Idriss IM, Andrus RD, Arango I, Castro G, Christian JT, Dobry R, Finn WDL, Harder LF, Hynes ME, Ishihara K, Koester JP, Liao SSC, Marcuson WF, Martin GR, Mitchell JK, Moriawaki Y, Power MS, Robertson PK, Seed RB, Stokoe KH. Liquefaction resistance of soils: summary report from the 1996 NCEER and 1998 NCEER/NSF workshops on evaluation of liquefaction resistance of soils. *J Geotech Geoenviron Eng*, ASCE 2001;127(10):817–33.
- [2] Moss RES, Seed RB, Kayen RE, Stewart JP, Youd TL, Tokimatsu K. Field case histories for CPT-based in situ liquefaction potential evaluation. *Geoengineering Research Rep*. UCB/GE-2003/04.
- [3] Idriss IM, Boulanger RW. *Soil Liquefaction During Earthquakes*. Earthquake Engineering Research Institute; 2008.
- [4] Boulanger RW, Idriss IM. CPT and SPT Based Liquefaction Triggering Procedures, Report No. UCD/CGM-14/01, University of California, Davis, April; 2014.
- [5] Robertson PK. Soil classification using the cone penetration test. *Can Geotech J* 1990;27(1):151–8.
- [6] Guo T, Prakash S. Liquefaction of Silts and Silt-Clay Mixtures. *J Geotech Geoenviron Eng* 1999;125(8):706–10. [Geotechnical Engineering, Chile].
- [7] Thevanayagam S, Shenthan T, Mohan S, Liang J. Undrained fragility of clean sands, silty sands, and sandy silts. *J Geotech Geoenviron Eng* 2002;128(10):849–59.
- [8] Thevanayagam S, Martin G. Liquefaction in silty soils—screening and remediation issues. *Soil Dyn Earthq Eng J* 2002;22(9–12):1035–42.
- [9] Bray JD, Sancio RB, Riemer MF, Durgunoglu HT. Liquefaction susceptibility of fine-grained soils. In: *Proceedings of 11th Inter. Conference On Soil Dynamics and Earthquake Engineering and 3rd Inter. Conference On Earthquake Geotechnical Engineering*, Doolin et al., Eds., Berkeley, 1, 655–662; 2004.
- [10] Xenaki VC, Athanasopoulos GA. Liquefaction resistance of sand – silt mixtures: an experimental investigation of the effects of fines. *Soil Dyn Earthq Engineering* 2003;23:183–94.
- [11] Prakasha KS, Chandrasekaran VS. Behavior of Marine Sand-Clay Mixtures under Static and Cyclic Triaxial Shear. *J Geotech Geoenviron Eng* 2005;131(2):213–22.
- [12] Bray JD, Sancio RB. Assessment of the liquefaction susceptibility of fine-grained soils. *J Geotech Geoenviron Eng*, ASCE 2006;132(9):1165–77.
- [13] Boulanger RW, Idriss IM. Liquefaction susceptibility criteria for silts and clays. *J Geotech Geoenviron Eng*, ASCE 2006;132(11):1413–26.
- [14] Taylor ML, Cubrinovski M, Haycock I. Application of new Gel-push sampling procedure to obtain high quality laboratory tests data for advanced geotechnical analyses. In: *Proceedings of the 2012 NZSEE Conference*, Paper No. 123, 1–8; 2012.
- [15] Umehara Y, Chiaro G, Kiyota T, Hosono Y, Yaguira Y, Chiba H. Effectiveness of ‘Gel-Push’ sampling technique to retrieve undisturbed sandy specimens for liquefaction test. In: *Proceedings of the 6th International Conference on Earthquake Geotechnical Engineering*, Nov. 1–4, Christchurch, New Zealand, pp.8; 2015.
- [16] Lee WF, Ishihara K, Chen CC. Liquefaction of silty sand—preliminary studies from Taiwan, New Zealand, and Japan earthquakes. In: *Proceedings of the international symposium on engineering lessons learned from the 2011 great east Japan earthquake*; 2012, pp. 747–758.
- [17] Stringer M, Taylor ML, Cubrinovski M. Advanced soil sampling of silty sands in Christchurch, Research report 2015-06, Civil and Natural Resources Engineering, ISSN: 1172–9511; 2015.
- [18] Al Atik L, Sitar N. Experimental and Analytical Study of the Seismic Performance of Retaining Structures, PEER Report 2008/104; 2008.
- [19] Mikola RG, Sitar N. Seismic earth pressures on retaining structures in cohesionless soils, Report No. UBC GT 13-01; 2013.
- [20] Erken A, Ulker BMC. Effect of cyclic loading on monotonic shear strength of fine-grained soils. *Eng Geol* 2007;89:243–57.
- [21] Wijewickreme D, Sanin MV. Cyclic Shear Loading Response of Fraser River Delta Silt. In: *Proceedings of 13th World Conference on Earthquake Engineering*, Vancouver, BC, Canada, 10 Pages.
- [22] Donahue JL, Bray JD, Riemer M. Liquefaction testing on fine-grained soils prepared using slurry deposition. In: *Proceedings of the 4th International Earthquake Geotechnical Engineering*, Thessaloniki, Greece, Paper 1226; 2007.
- [23] Arulmoli K, Muraleetharan KK, Hossain MM, Fruth LS. VELACS: Verification of Liquefaction Analyses by Centrifuge Studies—Laboratory Testing Program, Soil Data Report, Earth Technology Corporation, 1992; 1992.
- [24] Itasca Consulting Group Inc., Fast Lagrangian Analysis of Continua (FLAC2D) version 7.0; 2013.
- [25] Beaty M, Byrne PM. An Effective Stress Model for Predicting Liquefaction Behavior of Sand. In: *Proceedings of a Specialty Conference, Geotechnical Earthquake Engineering and Soil Dynamics*, ASCE 1998 pp. 766–777, Seattle.
- [26] Boulanger RW, Ziotopoulou K. Formulation of a sand plasticity plane-strain model for earthquake engineering applications. *J Soil Dyn Earthq Eng*, Elsevier 2013;53:254–67.
- [27] Ziotopoulou K, Boulanger RW. Calibration and implementation of a sand plasticity plane-strain model for earthquake engineering applications. *J Soil Dyn Earthq Eng* 2013;53:268–80.
- [28] Giannakou A, Travarasrou T, Ugalde J, Chacko J, Byrne P. Calibration Methodology for Liquefaction Problems Considering Level and Sloping Ground Conditions. In: *Proceedings of the 5th International Conference on Earthquake Geotechnical Engineering*, Santiago, Chile, Paper No. CMFGI; 2011.
- [29] Seed HB, Peacock WH. Test procedures for measuring soil liquefaction characteristics. *J Soil Mech Found Div*, ASCE 1971;97(SM8):1099–119.
- [30] Ishihara K, Iwamoto S, Yasuda S, Takatsu H. Liquefaction of anisotropically consolidated sand. In: *Proceedings of the 9th International Conference on Soil Mechanics and Foundation Engineering*, Japanese Society of Soil Mechanics and Foundation Engineering, Tokyo, Japan 2, 1977, pp. 261–264.
- [31] Finn WDL, Pickering DJ, Bransby PL. Sand liquefaction in triaxial and simple shear tests. *J Soil Mech Found Div*, ASCE 1971;97(SM4):639–59.
- [32] Ishibashi I, Sherif M. Soil liquefaction by torsional simple shear device. *J Geotech Eng Div*, ASCE 1974;100(GT8):871–88.
- [33] Castro G. Liquefaction and cyclic mobility of saturated sands. *J Geotech Eng Div*, ASCE 1975;101(GT6):551–69.
- [34] Seed HB. Soil liquefaction and cyclic mobility evaluation for level ground during earthquakes. *J Geotech Eng Div*, ASCE 1979;105(GT2):201–55.
- [35] Boulanger RW, Meyers MW, Mejia LH, Idriss IM. Behavior of a fine-grained soil during the Loma Prieta earthquake. *Can Geotech J* 1998;35:146–58.
- [36] Sancio RB. Ground failure and building performance in Adapazari, Turkey Ph.D. Thesis Berkeley: University of California; 2003.
- [37] Kokusho T. Water film in liquefied sand and its effect on lateral spread. *J Geotech Eng*, ASCE 1999;125(10):817–26.
- [38] Tokimatsu K, Taya Y, Zhang JM. Effects of pore water redistribution on post-liquefaction deformation of sands. In: *Proceedings of the 15th International Conference on Soil Mechanics and Geotechnical Engineering*, Balkema, Rotterdam, The Netherlands, 1, 289–292; 2001.
- [39] Kokusho T. Current state of research on flow failure considering void redistribution in liquefied deposits. *Soil Dyn Earthq Eng* 2003;23(7):585–603.
- [40] Kamai R, Boulanger RW. Simulations of a centrifuge test with lateral spreading and void redistribution effects. *J Geotech Geoenviron Eng*, ASCE 2013;139(8):1250–61.
- [41] Iai S. Performance of port structures during earthquakes. In: *Proceedings of 3rd International Conference on Performance-based Design in Earthquake Geotechnical Engineering (PBD-III)*, Vancouver, BC, Canada; 2017.
- [42] Kulasingam R, Malvick EJ, Boulanger RW, Kutter BL. Strength loss and localization at silt interlayers in slopes of liquefied sand. *J Geotech Geoenviron Eng*, ASCE 2004;130:1192–202.
- [43] Sento N, Kazama M, Uzuoka R, Hirofumi Ohmur H, Makoto Ishimaru M. Possibility of post liquefaction flow failure due to seepage. *J Geotech Geoenviron Eng*, ASCE 2004;130:707–16.
- [44] Malvick EJ, Kutter BL, Boulanger RW, Kulasingam R. Shear localization due to liquefaction-induced void redistribution in a layered infinite slope. *J Geotech Geoenviron Eng*, ASCE 2006;132(10):1293–303.